Ca^{2+}-activated Cl^- channel currents in mammary secretory cells from lactating mouse

Akihiro Kamikawa[1], Osamu Ichii[2], Junpei Sakazaki[1], Toru Ishikawa[1]

A.K. and T.I. conceived the project, designed the experiments, and wrote the manuscript. A.K., O.I., and J.S. performed the experiments and analyzed the data.

[1]Department of Basic Veterinary Medicine, Obihiro University of Agriculture and Veterinary Medicine, Obihiro, Japan

[2]Laboratory of Anatomy, Department of Biomedical Sciences, Graduate School of Veterinary Medicine, Hokkaido University, Sapporo, Japan.

Running Head: CaCC in mouse mammary secretory cell

Corresponding Author: Akihiro Kamikawa
Department of Basic Veterinary Medicine, Obihiro University of Agriculture and Veterinary Medicine, Inada-cho, Obihiro, Hokkaido, 080-8555, Japan
E-mail: akami@obihiro.ac.jp
Tel: +81-155-49-5355, Fax: +81-155-49-5371

Abstract

The Cl^- secretion via Ca^{2+}-activated Cl^- channel (CaCC) is critical for fluid secretion in exocrine glands like the salivary gland. Also in the mammary gland, it has been hypothesized that CaCC plays an important role in the secretion of Cl^- and aqueous phase of milk. However, there has been no evidence for the functional expression of CaCC in native mammary secretory (MS) cells of lactating animals. We therefore assessed the membrane current in the MS cells that were freshly isolated from lactating mice using the whole-cell patch-clamp techniques. In the MS cells, we detected the CaCC current that exhibited the following characteristics: 1) Ca^{2+}-dependnet activation at the concentrations of submicromolar range, 2) voltage-dependent activation, 3) slow kinetics for activation and deactivation, 4) outward rectification of the steady-state current, 5) anion permeability in the sequence of $I^- > NO_3^- > Br^- > Cl^- >>$ glutamate, 6) inhibition by Cl^- channel blockers (NFA, DIDS, and CaCCinh-A01). These characteristics of the native CaCC current were similar to reported characteristics of heterologously expressed TMEM16A. RT-PCR analyses showed the expression of multiple CaCC channels including TMEM16A, Best1, and Best3 in the mammary glands of lactating mice. Immunohistochemical staining revealed the localization of TMEM16A protein at the apical membrane of the MS cells. Collectively, our data strongly suggest that MS cells functionally express CaCC, which is at least partly constituted by TMEM16A. The CaCC such as TMEM16A at the apical membrane of the MS cells may influence the quantity and/or quality of milk.

Introduction

Mammary gland is an exocrine gland that is physiologically active only in postpartum female mammals. During the lactation period, mammary secretory (MS) cells produce milk containing organic components and ions. Lactose, one of the organic components, is a major osmolyte in milk, and contributes the determination of milk volume by influencing water secretion (43, 45). Meanwhile, because the ions substantially contribute to the osmolality of milk, it is also believed that the ion transport through the transcellular pathway involves in the secretion of ionic fluid and thus the regulation of amount and composition of milk, (41). Revealing the ion transport system in the MS cells is important for understanding the mechanisms of lactation.

As seen in other exocrine glands like the salivary gland and pancreatic exocrine gland (15, 22, 27), it has been considered that the transepithelial Cl^- secretion pathway, which is composed of basolateral transporters for Cl^- uptake and apical Cl^- channels for the excretion, might be present for the ionic fluid secretion in the mammary gland (41). Some findings have provided indirect evidence to support this notion. The molecular expression and/or function of Na^+-K^+ ATPase at the basolateral membrane of acinar cells have been shown in the lactating mammary gland (41). Na^+-K^+-Cl^- cotransport activity has been also demonstrated in mammary tissue explants (40). In addition, Na^+-K^+-Cl^- cotransporter 1 protein has been detected on the basolateral membrane of mammary acini of lactating mice, albeit at a lower level than ductal cells in virgin mice (42). These transporters may accumulate Cl^- inside the acinar cells, so that the calculated equilibrium potential of Cl^- across the apical membrane is more positive than their membrane potentials (24, 41). Although an agonist-stimulated secretion of the ionic fluid of milk has not been proven *in vivo*, in the experiment using a cultured mouse mammary epithelial cell line, addition of ATP to the basolateral and apical side of the cells augmented the transepithelial potential (apical side negative) and fluid secretion concomitant with the elevation of intracellular Ca^{2+} concentration (5). These changes were inhibited by the apical treatment of Cl^- channel inhibitor, 4,4'-diisothiocyanostilbene-2,2'-disulfonic acid (DIDS) (5), suggesting

69 that the Cl^- secretion via apical Ca^{2+}-activated Cl^- channel (CaCC) is important for ion secretion
70 and the subsequent osmotic water secretion under the situation where the intracellular Ca^{2+} is
71 elevated. Therefore, apical Cl^- channels, especially CaCCs, might be key molecules in the
72 mechanism of Cl^- and ionic fluid secretion in lactating mammary epithelia.

73 The current of the CaCC was first described in 1980s in *Xenopus* oocytes and inner
74 segments of salamander photoreceptor (2, 3, 28). Similar channels are expressed in various
75 mammalian epithelial cells including airway, intestinal, salivary gland, and pancreatic epithelia,
76 and contribute to the fluid secretion (13, 27). The CaCC, also called a "classical" CaCC, was
77 characterized by its distinctive properties; the activation with intracellular Ca^{2+} at
78 submicromolar range, the time-dependent activation and deactivation at positive and negative
79 membrane potentials, respectively, the outward rectification, the permeability to other
80 monovalent anions, and the sensitivities to Cl^- channel blockers (NFA, DIDS etc.) (13). Recent
81 studies identified TMEM16A, which is encoded by Ano1 gene, as the molecular basis of the
82 classical CaCC (6, 39, 48). Heterologously expressed TMEM16A displayed
83 electrophysiological characteristics that were similar to those of the classical CaCC (14, 35). In
84 salivary and pancreatic exocrine glands, TMEM16A expresses at the apical membrane of the
85 acinar cells (16, 48). *In vivo* knockdown and knockout of TMEM16A in mouse salivary gland
86 have clearly demonstrated that TMEM16A contributes to the CaCC currents and the
87 Ca^{2+}-mobilizing agonists-induced salivation (7, 38, 48). Thus, it is now known that TMEM16A
88 is a key molecule for the Ca^{2+}-dependent Cl^- and subsequent water secretion in the exocrine
89 glands (15, 35). The expression of *Ano1* mRNA has been detected in mouse mammary
90 epithelial cells at the late stage of pregnancy (39). However, the functional expression of CaCC
91 in native MS cells of lactating animals remains unclear.

92 We hypothesized that CaCCs like TMEM16A are active at the apical membrane of MS
93 cells of lactating animals. To test this hypothesis, in this study, we measured a whole-cell Cl^-
94 current that was activated by the physiological concentration of internal Ca^{2+} in the freshly
95 isolated MS cells of lactating mice and analyzed its properties to explore the molecular basis of

the CaCC current in the MS cells. Furthermore, we analyzed the expression of CaCCs using RT-PCR and immunohistochemistry. Our data strongly suggest that the classical CaCC is active in the MS cells and that TMEM16A at the apical membrane of the MS cells may partly contribute to the CaCC current.

Materials and methods

Animals

Female and male C57BL/6J mice obtained from Nihon SLC (Shizuoka, Japan) and their offspring were used for the experiments. The animal experimental procedures were carried out in accordance with Regulations on Management and Operation of Animal Experiments at the Obihiro University of Agriculture and Veterinary Medicine (OUAVM), and were approved by OUAVM Animal Care and Use Committee. The mice were housed at 23 ± 2°C with a 12 h: 12 h light: dark cycle, and given food and water *ad libitum*.

Patch-clamp experiment

The MS cells were isolated as detailed in our recent work (20). In brief, female mice were killed by cervical dislocation at mid-lactation (day 15.3 ± 0.2 of lactation, n=57) and their abdominal, inguinal, and/or thoracic mammary glands were collected. The minced mammary glands were incubated in a digestion buffer, which is a divalent cation-free standard bath solution containing (in mM) 145 NaCl, 5 KCl, 10 HEPES, 10 glucose, and 4.6 NaOH at pH 7.4, supplemented with collagenase (type I, 300 U/ml; Wako, Osaka, Japan) and hyaluronidase (100 U/ml; Sigma-Aldrich, St.Louis, MO), for 30 min at 37 °C in a shaking water bath. After gentle trituration with a pipette, the tissue was incubated once more for 30 min in the fresh digestion buffer. The digested tissue was filtered through 100 μm nylon mesh and washed three times with the divalent cation-free standard bath solution.

The isolated MS cells were plated out onto a coverslip in a chamber mounted on an inverted microscope and perfused with a standard bath solution of the following composition (in mM): 145 NaCl, 5 KCl, 10 HEPES, 10 glucose, 1 $CaCl_2$, 1 $MgCl_2$, and 4.6 NaOH at pH7.4. Current recordings were performed with an EPC7 Plus amplifier (HEKA Electronik, Lambrecht, Germany) in the whole-cell configurations. The reference electrode was a Ag-AgCl electrode, which was connected to the bath via an agar bridge filled with the standard bath solution. Patch-clamp pipettes were pulled from glass capillaries (G-1.5; Narishige, Tokyo, Japan) using

a vertical puller (Model PP-830; Narishige) so as to have resistances of 10-20 MΩ when filled with a nominally Ca^{2+}-free pipette solution (in mM): 90 NMDG-glutamate, 29 NMDG-Cl, 10 HEPES, 10 EGTA, 10 Glucose, 1 $MgCl_2$ (0.51 free Mg^{2+} calculated with WEBMAXC Standard), and 28 NMDG at pH7.4. The free Ca^{2+} concentrations of the pipette solutions were varied between 0.1 and 2 μM by adding an appropriate amount of $CaCl_2$ to the solutions (calculated with WEBMAXC Standard). The total Cl^- concentrations in the pipette solutions were adjusted to 31 mM. After preparing the whole-cell configuration, whole-cell currents were measured in a bath solution richly containing NMDG-Cl (NMDG-Cl bath solution) (in mM): 150 NMDG-Cl, 10 HEPES, 10 glucose, 1 $CaCl_2$, 1 $MgCl_2$, and 4.3 NMDG at pH7.4. In the experiments where anion selectivity was estimated, 150 NMDG-Cl in the NMDG-Cl bath solution was replaced by 150 NMDG-Br, 150 NMDG-I, 150 NMDG-NO_3, or 150 NMDG-glutamate.

The whole-cell currents were filtered at 1 kHz with an internal four-pole Bessel filter, sampled at 2 kHz, and stored directly on the computer's hard disk through the PowerLab (AD Instruments, Sydney, Australia). For whole-cell current measurements, the amplifier was driven by Scope software (AD Instruments) to allow the delivery of voltage-step or voltage-ramp protocols with concomitant digitization of the current. Membrane potential was held at −45 mV at resting. Current–voltage (*I–V*) relations were studied using a 400-ms step pulse (commanded from −105 mV to +95 mV, with 20-mV, and 3-s intervals) followed by a 400-ms tail potential of −105 mV, a 800-ms ramp pulse (commanded from −105 mV to +45 mV) with a 200-ms prepulse at -105 mV or a 1000-ms ramp pulse (commanded from −105 mV to +95 mV). The capacitance transient current was compensated. The cell capacitance was 19.9 ± 0.4 pF (n = 113). The average series resistance (R_s), which was 31.5 ± 0.5 MΩ (n =113), was not electrically compensated. Therefore, the conductance of currents were underestimated as a result of the voltage decrease across the R_s, and the command voltages were not corrected for this, except where conductances of tail currents were examined (Fig. 1J). For data analysis and/or graphical display, the digital data was processed with Excel (Microsoft, Redmond, WA)

and Igor Pro (WaveMetrics, Lake Oswego, OR). The pipette potential was corrected for the liquid junction potential between the pipette solution and the external solution, and between the external solution and the agar bridge, as described elsewhere (30). Briefly, the reference electrode was connected to the bath with 3M KCl-containing agar bridge and the potential differences between the standard bath solution filled in a pipette and other solutions perfused in the bath were measured in a current clamp mode of the EPC7 Plus amplifier.

Niflumic acid (NFA; dissolved in DMSO at 300 mM) and CaCCinh-A01 (dissolved in DMSO at 100 mM) were appropriately diluted by the NMDG-Cl bath solution. DIDS was dissolved in the NMDG-Cl bath solution on the day of the study. NFA, CaCCinh-A01, DIDS, HEPES, and EGTA were obtained from Sigma-Aldrich.

All experiments were performed at room temperature (~ 25 °C). Bath solution changes were accomplished by gravity feed from reservoirs. The results are reported as means ± SE (standard error of the mean) of independent experiments (n), where n refers to the number of cells patched.

Data analysis

In the experiment where the activation kinetics were analyzed, current traces from 10 to 390 ms of the 400-ms step pulses were fitted to the single exponential function of time (t) plus a constant term equation: $I(t) = A \exp(-t/\tau) + C$, where A and C are constant terms and τ is the time constant of activation. When the Cl^- conductance (g_{Cl}) of the tail current was determined, the voltage drops of prepulse potentials and tail potentials due to the series resistance were mathematically collected. The conductance was determined using the following equation; $g_{Cl} = I_{tail} / (E_{Cl} - V_{tail})$, where I_{tail}, E_{Cl}, and V_{tail} represent the tail current density, the equilibrium potential of Cl^-, and the corrected tail potential, respectively.

In the experiment where the permeability ratio (P_X/P_{Cl}) was estimated, the currents were elicited with the 800-ms ramp pulse {from (V_{hold} − 60) mV to (V_{hold} + 90) mV, where V_{hold} is a holding potential}. Because of the difference of the liquid junction potentials, the values of V_{hold}

were varied among the bath solutions containing different anions; −45 mV for Cl^- and I^-, −44 mV for Br^- and NO_3^-, and −39 mV for glutamate. And the permeability ratio (P_X/P_{Cl}) was calculated from the shift of the reversal potential (ΔV_{rev}) after substitution of most of the extracellular Cl^- by foreign anions (Br^-, I^-, NO_3^-, and glutamate). On the basis of the assumption that the current was only carried by these monovalent anions, ΔV_{rev} was formulated as follows (a derivation from Goldman, Hodgkin, and Katz equation): $\Delta V_{rev} = RT/F \ln \{P_{Cl} {}^1[Cl^-]_o / (P_{Cl} {}^2[Cl^-]_o + P_X {}^2[X^-]_o)\}$. Hence, $P_X/P_{Cl} = \{{}^1[Cl^-]_o - \exp(\Delta V_{rev} F/RT) {}^2[Cl^-]_o\} / \{\exp(\Delta V_{rev} F/RT) {}^2[X^-]_o\}$, where R, T, and F are the gas constant, absolute temperature, and Faraday constant, respectively, ${}^1[Cl^-]_o$ is the original extracellular Cl^- concentration, and ${}^2[Cl^-]_o$ and ${}^2[X^-]_o$ are the extracellular concentrations of Cl^- and the foreign anion X^-, respectively, after the replacement of the external solution. To examine the sensitivity of inhibitors, the whole-cell currents elicited by 0.6 μM Ca^{2+}-containing pipette solution were recorded using the 1000 ms-ramp pulse in the NMDG-Cl bath solution with or without inhibitors. The inhibited current at +90 mV was normalized by the current at +90 mV before the addition of inhibitors. The mean values of the normalized current (I_{norm}) were fitted to the Hill equation: $I_{norm} = I_{min} + (1 - I_{min}) / \{1 + ([Inh] / K_d)^h\}$ where h is the Hill coefficient, I_{min} is estimated I_{norm} at full-inhibition, [Inh] is the molar concentration of inhibitors applied, and K_d is the concentration at which one-half of the current is blocked.

Analyses of mRNA expression

Mammary glands were collected from lactating female mice at 15 - 18 day of lactation. Brain and testis were also collected from male mice for a positive control of the amplification of *Ano2*, *Ano1* (Δ*c*), and *Best2*. The collected tissues were immersed in RNAlater (Life Technologies, Carlsbad, CA) and stored at −80°C until used. RT-PCR analyses were performed as described previously (20). In brief, the total RNA was extracted from the tissues with Trizol (Life Technologies, Carlsbad, CA) and was cleaned-up with RNeasy kit (QIAGEN, Hilden, Germany) following the manufacturers' instructions. The total RNA (2 μg) was reverse

transcribed with oligo dT and Moloney murine leukemia virus reverse transcriptase (Promega, Madison, WI). PCR amplification was performed with Taq polymerase (Promega) and specific primer pairs. The sense and antisense primers used for the detection of CaCC transcripts (*Ano1*, *Ano2*, *Best1*, *Best2*, and *Best3*) and *Actb* are listed in Table 1. Primers for the check of mAno1 variants are listed in Table 2. The binding sites of primers in *Ano1* were summarized in Fig. 4A. The mixtures for PCR were subjected to 94°C for 2 min followed by 30 or 35 cycles of 30 s at 94°C, 30 s at 57°C, and 30 or 60 s at 72°C, and finally incubated at 72°C for 5 min. The PCR products were electrophoresed on 2% agarose gels containing ethidium bromide and visualized by UV light. For semi-quantitative analyses of mRNA expression level, the densities of the bands in digitized images were analyzed using the Image J software (ver1.48; National Institute of Health, Bethesda, MD, USA). In the nested PCR experiment, the DNA amplified in the first PCR was extracted from agarose gel after electrophoresis with the Quantum Prep Freez 'N Squeeze DNA Gel Extraction Spin Column (BIO RAD, Hercules, CA), and the extracted DNA was used for the second PCR with nested primers.

Immunohistochemical staining for TMEM16A

Sample preparation and immunostaining were performed as described in the previous study (21). Briefly, lactating mice were killed by exsanguination from the excised right atrium under deep anesthesia with an intraperitoneal injection of pentobarbital (0.2 mg/g body weight). Then, the 4% paraformaldehyde fixative was perfused from the left ventricle. The fixed abdominal mammary glands were dehydrated in alcohol, embedded in paraffin, and sliced into 3-μm-thick sections. For antigen retrieval, the sections were heated at 105°C for 15 min in 20 mM Tris-HCl buffer (pH 8.0) after deparaffinization. The sections were incubated with anti-TMEM16A antibody (1: 800; ab53212, Abcam) or control rabbit IgG (Santa Cruz Biotechnology, Dallas, TX, USA) overnight at 4°C, and then incubated with biotin-conjugated anti-Rabbit IgG and horseradish peroxidase-conjugated streptavidin (Nichirei, Tokyo, Japan). The sections were incubated with 3,3′-diaminobenzidine (DAB) tetrahydrochloride-H_2O_2

235 solution and Mayer's hematoxylin for the signal development and counter staining, respectively.
236 To determine the occurrences of the highly positive cells, the MS cells (> 1,000 cells per
237 mouse) were manually counted from randomly selected fields.
238
239 **Statistics**
240 Data are expressed as mean ± SE. Statistical analysis of the data was performed using a
241 Welch's t-test. *p* values less than 0.05 were considered statistically significant.
242
243

Results

Ca^{2+}-activated Cl^- current in MS cells

To clarify the functional expression of the CaCC in the MS cells, we analysed the whole-cell currents of the MS cells that were freshly isolated from lactating mouse mammary glands. In whole-cell patch-clamp experiments, the MS cells were perfused with the bath solution richly containing NMDG-Cl and with the pipette solution containing NMDG-glutamate and NMDG-Cl with the various concentrations (0 - 1 μM) of free Ca^{2+} ($[Ca^{2+}]_{pipette}$). The bath and the pipette solutions contained Cl^- at the concentrations of 154 and 31 mM, respectively. K^+ and Na^+ in the perfusate were substituted by an organic monovalent cation, NMDG, to reduce cation currents and to clearly detect a Cl^- current, because we have shown that MS cells exhibit an inwardly rectifying potassium channel (Kir) 2.1-like potassium current and a cation current that has not yet been fully characterized (20). The currents were elicited by stepping to various test pulses ranging from −105 to +95 mV with 20 mV intervals from the holding potential of −45 mV, followed by the hyperpolarized tail voltage (−105 mV) (Fig. 1A). When the MS cells were perfused with the nominally Ca^{2+}-free pipette solution, the cells showed only small currents (Fig. 1B). At 0.1 μM $[Ca^{2+}]_{pipette}$, which lies in the range of basal intracellular Ca^{2+} level (10, 46), approximately 67% (4 out of 6 cells tested) of the MS cells exhibited time-dependently activated outward currents at positive test potentials more than +35 mV, but little inward current at negative test potentials, as shown in Fig. 1C. The traces of the activated currents were fitted with a single exponential function with time constants of 399 ± 75, 370 ± 106, 346 ± 82, and 445 ± 126 ms at +35, +55, +75, and +95 mV, respectively (n = 4 each). When the cells were perfused with the pipette solution containing 1 μM free Ca^{2+}, the currents were further activated. Most cells showed the time-dependent activation and deactivation at depolarized and hyperpolarized test potentials, respectively (Fig. 1D). At 1 μM $[Ca^{2+}]_{pipette}$, approximately 88% (21 out of 24 cells) of the cells exhibited time-dependent activation with time constants of 78 ± 16, 78 ± 7, 75 ± 6, and 73 ± 5 ms at +35, +55, +75, and +95 mV, respectively. The membrane time constant arisen from series resistance and capacitance (< 1ms) was much smaller than the

activation τ. Because the other cells (3 out of 24 cells) showed promptly activated outward currents, their traces could not be fitted with a single exponential function. Thus, the activation kinetics at 1 μM $[Ca^{2+}]_{pipette}$ were faster than at 0.1 μM $[Ca^{2+}]_{pipette}$, and those were not affected by the membrane potentials. The deactivated traces at -105 mV of 19 cells out of 24 cells at 1 μM $[Ca^{2+}]_{pipette}$ were successfully fitted with a single exponential function with a time constant of 58.4 ± 3.8 ms. Due to the time-dependent changes, the steady-state current showed stronger outward rectification as compared to the instantaneous current (Fig. 1F).

Figure 1G summarizes the relationships between averaged steady-state currents and test potentials at various $[Ca^{2+}]_{pipette}$. The inset of Fig. 1G displays a Ca^{2+} (1 μM)-dependent current that was determined by subtracting the averaged current at nominally zero $[Ca^{2+}]_{pipette}$ from the averaged current at 1 μM $[Ca^{2+}]_{pipette}$. The elevating concentrations of the intracellular Ca^{2+} in the submicromolar range activated the outwardly rectifying currents (Fig. 1G). The reversal potentials (V_{rev}) of the instantaneous and steady-state current at 1 μM $[Ca^{2+}]_{pipette}$ (approximately −39 mV; Fig. 1F) and the Ca^{2+} (1 μM)-dependent current (approximately -37 mV; Fig. 1G, inset) were close to the E_{Cl} (−41 mV). Furthermore, the replacement of external Cl^- by glutamate decreased the current conduction and abolished the time-dependent outward current (Fig. 1E). Therefore, the Ca^{2+}-activated currents were carried by Cl^-. Our data demonstrated that the MS cells exhibit the Ca^{2+}-activated Cl^- current ($I_{Cl\text{-}Ca}$) and suggested that the cells functionally express the CaCC.

We further examined the voltage and Ca^{2+} dependency of the $I_{Cl\text{-}Ca}$ by analyzing the tail-currents that were elicited by the tail potentials of −105 mV after the test pulses (prepulses) raging from −105 mV to +95 mV (Fig. 1A). As shown in Fig. 1D, the cells activated by 1 μM $[Ca^{2+}]_{pipette}$ showed remarkable inward tail currents, which were transiently evoked and were gradually decreased due to the time-dependent deactivation of the CaCC. The instantaneous amplitude of the tail current represents the channel activity at the prepulse potential. Plots of the tail current amplitudes at different $[Ca^{2+}]_{pipette}$ *versus* the membrane potentials of the prepulses

297 are shown in Figure 1H. The cells perfused with nominally zero $[Ca^{2+}]_{pipette}$ displayed small tail
298 currents (approximately -2.5 pA/pF) after the hyperpolarized prepulses, which might be
299 associated with the Ca^{2+}- and voltage-independent current including unidentified background
300 currents (Fig. 1H). At the $[Ca^{2+}]_{pipette}$ of 0.1 μM and more, the tail currents were increased by the
301 positive prepulses (Fig. 1H), suggesting that the CaCC in the MS cell is activated in a
302 voltage-dependent manner. We next assessed the effect of internal free Ca^{2+} at different
303 prepulse potentials (Fig. 1I). The elevating concentration of $[Ca^{2+}]_{pipette}$ increased the tail
304 currents at every prepulse potentials, indicating the Ca^{2+}-dependent activation of CaCC in MS
305 cells. The Ca^{2+}-dependent activation at the positive membrane potentials was greater than that at
306 the negative potentials (Fig. 1I). This might suggest the interaction between Ca^{2+}-dependent and
307 voltage-dependent gating mechanisms. The findings obtained in electrophysiological analyses
308 should be interpreted with caution because our experiments where the series resistance was not
309 electrically compensated might have an error due to a voltage drop. To correct the error, we
310 determined the relationship between the membrane potentials of prepulses and tail current
311 conductances using the mathematically corrected actual membrane potentials (Fig.1J). The
312 corrected relationship also indicated the apparent Ca^{2+}- and voltage-dependent activation of the
313 $I_{Cl\text{-}Ca}$ in the MS cells (Fig.1J).
314 In our experiments, whole-cell currents activated with $[Ca^{2+}]_{pipette}$ more than 1 μM could
315 not be recorded with confidence because of the instability of the currents possibly due to the
316 resealing of a patched membrane. Therefore, we could not estimate the maximally activated
317 $I_{Cl\text{-}Ca}$, the dissociation constant (K_d) for Ca^{2+}, the voltage of half maximal activation ($V_{1/2}$), and
318 the relationship between the Ca^{2+} sensitivity and the voltage sensitivity in a quantitative manner.
319
320 To further characterize the $I_{Cl\text{-}Ca}$ in the MS cells, the permeability sequence of monovalent
321 anions was determined by replacing external Cl^- with I^-, NO_3^-, Br^-, or glutamate and by
322 measuring a V_{rev} shift in separate cells (Fig. 2A-D). For this experiment, the $I_{Cl\text{-}Ca}$ was activated
323 with the pipette solution containing 31 mM Cl^- and 1 μM Ca^{2+} and was elicited by the ramp

pulse protocol. In the bath solution containing 154 mM Cl^- and the solution cotaining150 mM I^-, NO_3^- or Br^- instead of 150 mM Cl^-, the MS cells showed the currents with slight outward rectifications (Fig. 2A-C). In the bath solution containing 150 mM glutamate, the MS cells showed a linear I-V relationship with small conductances (Fig. 2D). The replacement of external Cl^- with I^-, NO_3^-, Br^- and glutamate induced the shifts of V_{rev} by −16.3 ± 2.4 (n = 6), −14.0 ± 2.9 (n = 6), −8.4 ± 1.0 (n = 7), and +36.3 ± 6.6 (n = 7) mV, respectively, from the V_{rev} in the solution with 154 mM Cl^- (−35.8 ± 1.8 mV, n = 26). Using the Goldman, Hodgkin and Katz equation, the relative permeabilities of these monovalent anions (P_X/P_{Cl}) were estimated to be 1.94 ± 0.19, 1.79 ± 0.19, 1.40 ± 0.05 and 0.28 ± 0.09 for I^-, NO_3^-, Br^-, and glutamate, respectively (Fig. 2E). Furthermore, we compared the V_{rev} between the bath solution containing 150 mM NMDG-I and 150 mM NMDG-NO_3 in a single cell to confirm the difference of the permeabilities between I^- and NO_3^-. The V_{rev} in the NMDG-I solution was more negative than that in the NMDG-NO_3 solution in all the cells that we tested (−3.2 ± 1.3 mV, n = 4). These results revealed that the permeability sequence of the $I_{Cl\text{-}Ca}$ in the MS cells was $I^- > NO_3^- > Br^- > Cl^- >>$ glutamate.

Collectively, our findings suggested that the native MS cells functionally express the CaCC, which shows the Ca^{2+}-dependent activation at submicromolar concentrations, the voltage-dependent activation, the outward rectification of the steady-state *I-V* relationship, the slow kinetics for activation and deactivation, and the following permeability sequence to anions: $I^- > NO_3^- > Br^- > Cl^- >>$ glutamate. These characteristics of the CaCC in MS cells were similar to the classical CaCC recorded in various epithelial cells (13) and heterologously expressed TMEM16A (14, 35).

Pharmacological properties of Ca^{2+}-activated Cl^- current in MS cells

We next investigated the pharmacological properties of the $I_{Cl\text{-}Ca}$ in the MS cells. In this experiment, broad-spectrum classical Cl^- channel blockers including NFA and DIDS and a newly found CaCC-selective blocker, CaCCinh-A01 (29), were utilized. The currents were

activated by 0.6 μM $[Ca^{2+}]_{pipette}$ and recorded with the ramp pulse protocol (from -105 to +95 mV) at pre- and post-treatment of blockers (insets of Figs. 3A, B, D). The relationships between the averaged normalized current (I_{norm}) and membrane potentials were summarized (Figs. 3A, B, D). NFA at 100 μM effectively inhibited the $I_{Cl\text{-}Ca}$ (Figs. 3A). The I_{norm} at +90 mV were 0.93 ± 0.03, 0.79 ± 0.05, 0.40 ± 0.03, 0.18 ± 0.02, and 0.17 ± 0.07 with NFA at the concentrations of 0.01, 1, 10, 100, and 300 μM, respectively. And the K_d value of NFA for the $I_{Cl\text{-}Ca}$ at +90 mV was estimated to be 3.7 μM (Fig. 3C). DIDS inhibited the outward $I_{Cl\text{-}Ca}$ at the concentration of 3 mM (Fig. 3B). With DIDS at 10, 100, 300, 1000, and 3000 μM, the I_{norm} at +90 mV were 0.95 ± 0.02, 0.92 ± 0.01, 0.85 ± 0.09, 0.46 ± 0.08, and 0.21 ± 0.02, respectively. And the K_d value of DIDS was estimated to be 805 μM (Fig. 3C). The treatment of CaCCinh-A01 at the concentration of 100 μM suppressed the $I_{Cl\text{-}Ca}$ (70.3 ± 1.1% inhibition at +90 mV) (Fig. 3D). The effects of the blockers, especially CaCCinh-A01, were partially irreversible (Figs. 3A, B, D). The inhibitory effect of NFA and DIDS, but not CaCCinh-A01, showed a voltage dependency (Fig. 3E).

mRNA expression of CaCC in lactating mammary glands.

The electrophysiological and pharmacological analyses suggested the functional expression of CaCC, particularly TMEM16A, in the MS cells. Thus the expression of *Ano1* gene, which encodes TMEM16A, and other CaCC genes (*Ano2*, *Best1*, *Best2*, and *Best3*) were tested. The RT-PCR analyses showed the abundant expression of *Ano1* mRNA in the mammary glands of lactating mice (Fig. 4B). Additionally, *Best1* and *Best3*, but not *Ano2* and *Best2*, mRNA were detected in the lactating mammary glands (Fig. 4B).

It has been reported that human TMEM16A has multiple functional isoforms generated by the combination of alternative promoters and alternative three exons (35). The variant that lacks the first ATG (start codon; at 306-308 in the h*ANO1* sequence of accession number NM_018043.5) is translated into a protein lacking N-terminal amino acids sequence labeled segment *a*. And variants that include or skip the three alternative exons translated into the

variants with or without segment *b*, *c*, and *d*. Homologous variants were also reported in tissues of mouse (8, 17, 32). We therefore examined the mouse *Ano1* (m*Ano1*) variants that are expressed in the lactating mammary glands with the specific primer pairs (Table 2, Fig. 4A). First, the presence of m*Ano1* mRNA including the first ATG was assessed. We detected the 5' region harboring the start codon (ATG at 269-271 in the m*Ano1* sequence of accession number NM_178642.5) that corresponds to the first ATG in human *ANO1* (h*ANO1*) (Fig. 4C; primers S1 and A1). Next, three alternative spliced variants were examined. Primer pair spanning the exon encoding the segment *b* (exon *b*) amplified *b*-inclusion and *b*-skipping transcripts (Fig. 4C; primers S2 and A2). The semi-quantitative comparison by densitometry showed that the expression level of *b*-inclusion transcripts was approximately 1.3-fold (1.28 ± 0.13, n = 3) greater than that of *b*-skipping transcripts. The *c*-skipping variants were detected in brain but not in the lactating mammary glands (Fig. 4C; primers S6 and A5). When exon *d*-spanning primers used, abundant *d*-skipping transcripts and lesser *d*-inclusion transcripts (0.22 ± 0.12 in abundance relative to *d*-skipping transcripts) were amplified (Fig. 4C; primers S5 and A5). When the primer set of sense primer binding to the exon *b* (primer S4) and the antisense primer binding to the 3'-flanking region of exon *d* (primer A5) or the sense primer binding to the 5'-flanking region of exon *b* (primer S2) and the antisense primer binding to the exon *d* (primer A3) were utilized, *bc*Δ*d*, Δ*bcd*, and *bcd* fragments were amplified (Fig. 4C). Because the bands of the *bcd* variant were faint, we further confirmed their expression by using primer pairs for the nested PCR, S2 and A3 followed by S2 and A2 (Fig. 4C). Moreover, when the sense and antisense primers binding to *b*-skipping and *d*-skipping sequence, respectively, were used, we detected amplification (Fig. 4C; primer S3 and A4). These results showed that multiple *Ano1* transcripts encoding TMEM16A isoforms including at least TMEM16A (*ac*), (*abc*), (*acd*), and (*abcd*) are present in the mammary gland of lactating mice.

Protein expression of TMEM16A in lactating mammary gland

We next examined the localization of TMEM16A in the lactating mammary gland. As shown in Fig. 5A, the mammary glands of lactating mice were mainly occupied by a mammary parenchymal tissue such as lobuloalveolar and ductal structures. The secondary and/or tertiary ductal structures were surrounded by thick stroma like fibroblast and collagen fiber, while the lobuloalveolar tissues were surrounded by thinner stroma (Fig. 5A), as reported previously (37). The cuboidal luminal cells, that is MS cells, in both the acinar and ductal structures were enlarged with a large cytoplasm and some of the cells contained milk fat globules (Fig. 5). The sections were immunohistochemically stained with the anti-TMEM16A antibody (Figs. 5A, B) or the control IgG (Fig. 5C). The anti-TMEM16A antibody used in this experiment, that is generated using the human TMEM16A peptide (raging between aa 100-450) as an immunogen, detects multiple mTMEM16A variants, including *ab*, *ac* and *abc* variants, at the cell surface (11). A minor fraction of the epithelial cells (0.9 ± 0.2%, n = 3) were most densely stained at the cytosol region and the apical membrane (Figs. 5A, B; arrowheads). Such densely stained cells were small in their size with a narrow cytoplasm and did not include lipid droplets inside (Figs. 5A, B). Because of the low occurrence and the unusual shape, these types of cells were not used for patch-clamp analyses. The nature of the densely stained cells remains to be elucidated. Majority of the MS cells in both acinar and ductal structures displayed the positive reaction to anti-TMEM16A antibody at the apical membrane (Figs. 5A, B; arrows).─These results demonstrated that TMEM16A is expressed at the apical membrane of MS cells in the lactating mammary gland.

Discussion

It has been hypothesized that the Cl^- channel at the apical membrane of MS cells contributes to the Cl^- and subsequent water secretion into the lumen of the mammary gland. However, there is no direct evidence for the functional expression of Cl^- channels in the MS cells of lactating mammals. Here we first demonstrated the functional expression of CaCC in freshly isolated MS cells of lactating mice. The CaCC exhibited the following characteristics: 1) Ca^{2+}-dependnet activation, 2) voltage-dependent activation, 3) time-dependent activation and deactivation, 4) outward rectification of the steady-state current, 5) permeability ratios in the sequence of $I^- > NO_3^- > Br^- > Cl^- >>$ glutamate, 6) sensitivity to the Cl^- channel blockers such as NFA, DIDS, and CaCCinh-A01.

It has been well known that TMEM16A, one of CaCC molecules, plays important roles in the Cl^- secretion in exocrine glands (15, 35). To assess the possibility that the CaCC current in the MS cells might be conducted by TMEM16A, the electrophysiological and pharmacological characteristics of the MS-cell CaCC current were compared with the reported properties of TMEM16A and the classical CaCC. Firstly, the *I-V* relationship of the steady-state CaCC current in the MS cells showed an outward rectification due to the slow activation and deactivation at positive and negative membrane potentials, respectively (Figs. 1D, F), that agreed with the features of TMEM16A (14, 33, 35). However, a few MS cells (3 out of 24 cells at 1 μM $[Ca^{2+}]_i$) showed instantaneous activation and little time-dependent activation. This cell-to-cell variation in the activation kinetics might be due to the different ratio of TMEM16A variants in each of the MS cells, because Ferrera *et al*. (11) have shown that lack of segment *b* resulted in larger instantaneous current and smaller time-dependent activation. We actually detected both *b*-inclusion and -skipping variants in lactating mammary glands (Fig. 4C). Secondly, tail-current analyses showed that the CaCC in the MS cells was activated by intracellular Ca^{2+} at submicromolar concentrations (Figs. 1I). Because the activation level at 1 μM $[Ca^{2+}]_i$ did not reach the maximum level, the K_d value of the Ca^{2+}-dependent activation

451 would be > 300 nM at +95 mV in the MS cells. It has been revealed that the Ca^{2+}-sensitivity of
452 hTMEM16A (*ac*) (K_d = 85 nM at +100 mV) was nearly 4-hold higher than that of the
453 hTMEM16A (*abc*) variant (K_d = 332 nM at +100 mV) (11). Romanenko *et al*. have examined
454 the Ca^{2+}-sensitivity of mTMEM16A (*ac*) and calculated the K_d value as 196 nM at +120 mV.
455 Thus, the Ca^{2+}-sensitivity of the CaCC current in the MS cells may lie within the range of
456 mTMEM16A variants including (*ac*) and (*abc*). Lastly, the permeability sequence of the CaCC
457 in MS cells was determined as $I^- > NO_3^- > Br^- > Cl^- >>$ glutamate (Fig. 2E). These
458 characteristics were consistent with previous reports for the heterologously expressed
459 mTMEM16A (*ac*) (38), mTMEM16A (*0*) (31), and hTMEM16A (*ab*) (19).
460 The potency of classical Cl^- channel inhibitors, NFA and DIDS, for the CaCC current in
461 the MS cells was also similar to that for mammalian TMEM16A. Both drugs inhibited the $I_{Cl\text{-}Ca}$
462 in the MS cells, and the block by NFA (K_d = 3.7 μM at +90 mV) was more potent than DIDS
463 (K_d = 805 μM at +90 mV) in the MS cells (Figs. 3A-C). The higher potency of NFA compared
464 to DIDS has been also reported for heterologously expressed TMEM16A. For instance, the K_d
465 values of NFA and DIDS for hTMEM16A (*abc*) were 7.4 μM and 549 μM, respectively, at +80
466 mV (25). And mTMEM16A (*ac*) displays the higher sensitivity to NFA ($K_d \approx$ 30 μM) compared
467 to DIDS ($K_d \approx$ 300 μM) (38). In our experiment, the value of the Hill coefficient for NFA was
468 estimated to be 0.8, close to unity, likely indicative of pore block. On the other hand, the Hill
469 coefficient for DIDS was estimated to be 1.5. This does not exclude the possibility of the
470 presence of multiple binding sites for DIDS. Thus, there might be different blocking
471 mechanisms between NFA and DIDS for the CaCC in the MS cells. However, the precise
472 mechanism has not been elucidated in this study. Also for heterologously expressed mammalian
473 TMEM16A, the blocking mechanisms of these inhibitors have not been conclusively shown and
474 the value of the Hill coefficient for DIDS has not been available at present.
475 Collectively, the characteristics of the CaCC current in the MS cells were, at least
476 qualitatively, similar to those of TMEM16A variants (*ac*, *abc*, and *acd*). Thus, our data strongly
477 suggest that TMEM16A partly contributes to the CaCC current in the MS cells. Actually,

transcripts of these variants were detected in lactating mammary gland with RT-PCR analyses (Fig. 4C).

Do other CaCCs contribute to the $I_{Cl\text{-}Ca}$? It has been known that membrane proteins such as TMEM16B, Best1, Best2, and Best3 are activated with the submicromolar $[Ca^{2+}]_i$ and function as a CaCC (26, 36, 39, 44, 47). Because the mRNA expression of TMEM16B and Best2 was negligible in the mammary glands of lactating mice, it is likely that these two molecules have little involvement in the $I_{Cl\text{-}Ca}$ in the MS cells. The mRNA expressions of Best1 and Best3 were detected in the lactating mammary gland. However, the pharmacological properties of the CaCC in the MS cells were different from those of Best1 and Best3. Best1 has lesser sensitivity to NFA (K_d = 102 μM at +80 mV) and greater sensitivity to DIDS (K_d = 3.9 μM at +80 mV) than TMEM16A (25). Also, the current of a native Best3-like channel in mammalian cells was not inhibited by 100 μM NFA and was pharmacologically distinguishable from NFA (100 μM)-sensitive TMEM16A-like current (26). Thus, it is suggested that the contribution of Best1 and Best3 to the $I_{Cl\text{-}Ca}$ in the MS cells was small. However, the relatively higher permeability to glutamate (Fig. 2E) than heterologously expressed TMEM16A (34) and residual current after addition of NFA (100 μM) (Fig. 3A) may imply that Best currents were subtly included in the $I_{Cl\text{-}Ca}$ of the MS cells. Moreover, we cannot exclude the possibility that other unidentified currents such as a current at nominally zero $[Ca^{2+}]_i$ affected the analyses of properties of the native CaCC in the MS cells. The study using mammary gland-specific CaCCs (TMEM16A, Best1, or Best3) knockout mice would be helpful to further examine the contribution of these channels to the $I_{Cl\text{-}Ca}$ in the MS cells.

It is worth discussing the physiological significance of the CaCC in lactating mammary gland. The CaCC in the MS cells may contribute to the Ca^{2+}-activated Cl^- secretion and the subsequent osmotic water secretion, and may finally modulate the volume and composition of milk. Although such a stimulated secretion of the ionic fluid by the intracellular Ca^{2+}

505 recruitment in the MS cells has not been proven *in vivo*, the present study and previous reports
506 may support the validity of this secretion model. First, as shown in Figures 1H and I, the
507 activity of the CaCC in the MS cells was regulated at physiological levels of $[Ca^{2+}]_i$ at negative
508 membrane potentials, which are near the reported resting membrane potential of the apical
509 membrane (4, 23). It has been reported that the intracellular concentration of Ca^{2+} is elevated by
510 extracellular purine nucleotides, which is released by mechanical stress in autocrine and/or
511 paracrine manner in cultured mammary tumor cells (10). Thus, when the MS cells receive the
512 mechanical stress during the milk ejection process (i.e. acini contraction), the purine nucleotides
513 may elevate intracellular Ca^{2+} and then modulate the CaCC activity. However, we should note
514 that the role of the purinergic stimuli for the $[Ca^{2+}]_i$ elevation in the native MS cells remains
515 controversial (46). Secondly, TMEM16A, a convincing candidate of the CaCC in the MS cells,
516 was located at the apical membrane of the MS cells in lactating mammary glands (Fig. 5).
517 Based on the data of the intracellular $[Cl^-]$ {62 mM in guinea pig (23)} and milk $[Cl^-]$ {42 mM
518 in mice (18), 12 - 68 mM in guinea pig (1, 23)}, the equilibrium potential of Cl^- (E_{Cl}) at apical
519 membrane calculated to be from −2 to +44 mV. It is speculated that Cl^- has an outward
520 electrochemical driving force at the apical membrane because its membrane potential is
521 reported as −44 mV in guinea pig (23) and −14 mV in mice (4). Thus, Cl^- may be secreted to
522 the lumen when the apical TMEM16A is activated. It has been demonstrated that DIDS (0.5
523 mM)-sensitive CaCC contributes to the purinergically stimulated Cl^- secretion in the monolayer
524 culture of a mouse mammary epithelial cell line (4). This study is evidence for the
525 Ca^{2+}-stimulated secretion model in mammary epithelial cells. However, the inward current of
526 the native CaCC (i.e. Cl^- efflux) was not inhibited by 3 mM DIDS in the MS cells (Fig. 3E).
527 The CaCC shown in our study may be different from the channel reported in the cultured
528 mammary epithelial cells. Thirdly, the Kir2.1-like Kir channel (20) and the Ca^{2+}-activated K^+
529 channels (9, 12) were detected in the native MS cells and primary cultured mammary epithelial
530 cells, respectively. The potassium efflux through such potassium channels may contribute to
531 maintain the driving force for Cl^- secretion via the CaCC. Further studies will be necessary to

verify the Ca^{2+}-stimulated secretion model and its molecular basis in lactating mammary gland.

We should pay attention that the amount and composition of milk may not be accounted for solely by the ionic transport model proposed in other exocrine glands including the salivary and pancreatic gland because the mammary gland has distinctive features. Milk contains substantial carbohydrate including lactose (approximately 60 and 200 mM in mice and human, respectively) as an osmolyte. Thus, the carbohydrate secretion also affects the amount and composition of milk (43, 45). Moreover, because produced milk is stored in acini until it is suckled by pups, the milk composition can be modulated after production by the MS cells during the storage. Further studies will be needed to fully understand the molecular mechanisms where the composition of milk is determined. It has also been known that the ionic compositions of milk are varied among mammalian species (e.g. higher Cl^- concentration of milk in rodents than humans and ruminants), suggesting the difference of mechanisms for transepithelial ion secretion between species. Thus, investigating the difference of CaCC activity and its role in lactation between species will be of interest.

In conclusion, we have demonstrated the functional expression of CaCC in the MS cells freshly isolated from lactating mice. Our results strongly suggest that TMEM16A at lease partly contributes to the CaCC current in the MS cells. It would be of interest to investigate the role of TMEM16A-like CaCC in stimulated Cl^- and ionic fluid secretion in MS cells during lactation.

Acknowledgements

The authors would like to thank Dr. Daisuke Kondoh and Akie Hayashi for technical assistance in immunohistochemical and patch-clamp experiments, respectively.

Grant

This work was supported in part by the Akiyama Life Science Foundation and the Kuribayashi Ikuei Foundation.

560 **References**

561

562 1. Anderson RR, Sheffield LG. Macrominerals in guinea pig milk during 21 days of lactation.
563 J Dairy Sci. 1988;71(2):337-345.

564 2. Bader CR, Bertrand D, Schwartz EA. Voltage-activated and calcium-activated currents
565 studied in solitary rod inner segments from the salamander retina. J Physiol.
566 1982;331:253-284.

567 3. Barish ME. A transient calcium-dependent chloride current in the immature *Xenopus*
568 oocyte. J Physiol. 1983;342:309-325.

569 4. Berga SE. Electrical potentials and cell-to-cell dye movement in mouse mammary gland
570 during lactation. Am J Physiol. 1984;247(1 Pt 1):C20-25.

571 5. Blaug S, Rymer J, Jalickee S, Miller SS. P2 purinoceptors regulate calcium-activated
572 chloride and fluid transport in 31EG4 mammary epithelia. Am J Physiol Cell Physiol.
573 2003;284(4):C897-909.

574 6. Caputo A, Caci E, Ferrera L, Pedemonte N, Barsanti C, Sondo E, Pfeffer U, Ravazzolo R,
575 Zegarra-Moran O, Galietta LJ. TMEM16A, a membrane protein associated with
576 calcium-dependent chloride channel activity. Science. 2008;322(5901):590-594.

577 7. Catalán MA, Kondo Y, Peña-Munzenmayer G, Jaramillo Y, Liu F, Choi S, Crandall E,
578 Borok Z, Flodby P, Shull GE, Melvin JE. A fluid secretion pathway unmasked by
579 acinar-specific Tmem16A gene ablation in the adult mouse salivary gland. Proc Natl Acad
580 Sci U S A. 2015;112(7):2263-2268.

581 8. Davis AJ, Forrest AS, Jepps TA, Valencik ML, Wiwchar M, Singer CA, Sones WR,
582 Greenwood IA, Leblanc N. Expression profile and protein translation of TMEM16A in
583 murine smooth muscle. Am J Physiol Cell Physiol. 2010;299(5):C948-959.

584 9. Enomoto K, Furuya K, Maeno T, Edwards C, Oka T. Oscillating activity of a
585 calcium-activated K^+ channel in normal and cancerous mammary cells in culture. J Membr
586 Biol. 1991;119(2):133-139.

10. Enomoto K, Furuya K, Yamagishi S, Oka T, Maeno T. The increase in the intracellular Ca^{2+} concentration induced by mechanical stimulation is propagated via release of pyrophosphorylated nucleotides in mammary epithelial cells. Pflugers Arch. 1994;427(5-6):533-542.
11. Ferrera L, Caputo A, Ubby I, Bussani E, Zegarra-Moran O, Ravazzolo R, Pagani F, Galietta LJ. Regulation of TMEM16A chloride channel properties by alternative splicing. J Biol Chem. 2009;284(48):33360-33368.
12. Furuya K, Enomoto K, Furuya S, Yamagishi S, Edwards C, Oka T. Single calcium-activated potassium channel in cultured mammary epithelial cells. Pflugers Arch. 1989;414(2):118-124.
13. Hartzell C, Putzier I, Arreola J. Calcium-activated chloride channels. Annu Rev Physiol. 2005;67:719-758.
14. Hartzell HC, Yu K, Xiao Q, Chien LT, Qu Z. Anoctamin/TMEM16 family members are Ca^{2+}-activated Cl^- channels. J Physiol. 2009;587(Pt 10):2127-2139.
15. Hong JH, Park S, Shcheynikov N, Muallem S. Mechanism and synergism in epithelial fluid and electrolyte secretion. Pflugers Arch. 2014;466(8):1487-1499.
16. Huang F, Rock JR, Harfe BD, Cheng T, Huang X, Jan YN, Jan LY. Studies on expression and function of the TMEM16A calcium-activated chloride channel. Proc Natl Acad Sci U S A. 2009;106(50):21413-21418.
17. Hwang SJ, Blair PJ, Britton FC, O'Driscoll KE, Hennig G, Bayguinov YR, Rock JR, Harfe BD, Sanders KM, Ward SM. Expression of anoctamin 1/TMEM16A by interstitial cells of Cajal is fundamental for slow wave activity in gastrointestinal muscles. J Physiol. 2009;587(Pt 20):4887-4904.
18. Jost B, Vilotte JL, Duluc I, Rodeau JL, Freund JN. Production of low-lactose milk by ectopic expression of intestinal lactase in the mouse mammary gland. Nat Biotechnol. 1999;17(2):160-164.
19. Jung J, Nam JH, Park HW, Oh U, Yoon JH, Lee MG. Dynamic modulation of

614 ANO1/TMEM16A HCO_3^- permeability by Ca^{2+}/calmodulin. Proc Natl Acad Sci U S A.
615 2013;110(1):360-365.
616 20. Kamikawa A, Ishikawa T. Functional expression of a Kir2.1-like inwardly rectifying
617 potassium channel in mouse mammary secretory cells. Am J Physiol Cell Physiol.
618 2014;306(3):C230-240.
619 21. Kamikawa A, Sugimoto S, Ichii O, Kondoh D. Decrease in an Inwardly Rectifying
620 Potassium Conductance in Mouse Mammary Secretory Cells after Forced Weaning. PLoS
621 One. 2015;10(10):e0141131.
622 22. Lee MG, Ohana E, Park HW, Yang D, Muallem S. Molecular mechanism of pancreatic
623 and salivary gland fluid and HCO_3^- secretion. Physiol Rev. 2012;92(1):39-74.
624 23. Linzell JL, Peaker M. Intracellular concentrations of sodium, potassium and chloride in
625 the lactating mammary gland and their relation to the secretory mechanism. J Physiol.
626 1971;216(3):683-700.
627 24. Linzell JL, Peaker M. Mechanism of milk secretion. Physiol Rev. 1971;51(3):564-597.
628 25. Liu Y, Zhang H, Huang D, Qi J, Xu J, Gao H, Du X, Gamper N, Zhang H.
629 Characterization of the effects of Cl^- channel modulators on TMEM16A and bestrophin-1
630 Ca^{2+} activated Cl^- channels. Pflugers Arch. 2015;467(7):1417-1430.
631 26. Matchkov VV, Larsen P, Bouzinova EV, Rojek A, Boedtkjer DM, Golubinskaya V,
632 Pedersen FS, Aalkjaer C, Nilsson H. Bestrophin-3 (vitelliform macular dystrophy 2-like 3
633 protein) is essential for the cGMP-dependent calcium-activated chloride conductance in
634 vascular smooth muscle cells. Circ Res. 2008;103(8):864-872.
635 27. Melvin JE, Yule D, Shuttleworth T, Begenisich T. Regulation of fluid and electrolyte
636 secretion in salivary gland acinar cells. Annu Rev Physiol. 2005;67:445-469.
637 28. Miledi R. A calcium-dependent transient outward current in *Xenopus laevis* oocytes. Proc
638 R Soc Lond B Biol Sci. 1982;215(1201):491-497.
639 29. Namkung W, Phuan PW, Verkman AS. TMEM16A inhibitors reveal TMEM16A as a
640 minor component of calcium-activated chloride channel conductance in airway and

641 intestinal epithelial cells. J Biol Chem. 2011;286(3):2365-2374.
642 30. Neher E. Correction for liquid junction potentials in patch clamp experiments. In: Methods
643 in Enzymology, edited by Rudy B. San Diego, CA: Academic, 1992, vol 207, 123-131
644 31. Ni YL, Kuan AS, Chen TY. Activation and inhibition of TMEM16A calcium-activated
645 chloride channels. PLoS One. 2014;9(1):e86734.
646 32. O'Driscoll KE, Pipe RA, Britton FC. Increased complexity of *Tmem16a/Anoctamin* 1
647 transcript alternative splicing. BMC Mol Biol. 2011;12:35.
648 33. Ohshiro J, Yamamura H, Suzuki Y, Imaizumi Y. Modulation of TMEM16A-channel
649 activity as Ca^{2+} activated Cl^- conductance via the interaction with actin cytoskeleton in
650 murine portal vein. J Pharmacol Sci. 2014;125(1):107-111.
651 34. Park H, Han KS, Oh SJ, Jo S, Woo J, Yoon BE, Lee CJ. High glutamate permeability and
652 distal localization of Best1 channel in CA1 hippocampal astrocyte. Mol Brain. 2013;6:54.
653 35. Pedemonte N, Galietta LJ. Structure and function of TMEM16 proteins (anoctamins).
654 Physiol Rev. 2014;94(2):419-459.
655 36. Pifferi S, Dibattista M, Menini A. TMEM16B induces chloride currents activated by
656 calcium in mammalian cells. Pflugers Arch. 2009;458(6):1023-1038.
657 37. Richert MM, Schwertfeger KL, Ryder JW, Anderson SM. An atlas of mouse mammary
658 gland development. J Mammary Gland Biol Neoplasia. 2000;5(2):227-241.
659 38. Romanenko VG, Catalán MA, Brown DA, Putzier I, Hartzell HC, Marmorstein AD,
660 Gonzalez-Begne M, Rock JR, Harfe BD, Melvin JE. Tmem16A encodes the
661 Ca^{2+}-activated Cl^- channel in mouse submandibular salivary gland acinar cells. J Biol
662 Chem. 2010;285(17):12990-13001.
663 39. Schroeder BC, Cheng T, Jan YN, Jan LY. Expression cloning of TMEM16A as a
664 calcium-activated chloride channel subunit. Cell. 2008;134(6):1019-1029.
665 40. Shennan DB. Evidence for furosemide-sensitive Na^+-K^+- Cl^- co-transport in lactating rat
666 mammary tissue. Q J Exp Physiol. 1989;74(6):927-938.
667 41. Shennan DB, Peaker M. Transport of milk constituents by the mammary gland. Physiol

668 Rev. 2000;80(3):925-951.
669 42. Shillingford JM, Miyoshi K, Flagella M, Shull GE, Hennighausen L. Mouse mammary
670 epithelial cells express the Na-K-Cl cotransporter, NKCC1: characterization, localization,
671 and involvement in ductal development and morphogenesis. Mol Endocrinol.
672 2002;16(6):1309-1321.
673 43. Stacey A, Schnieke A, Kerr M, Scott A, McKee C, Cottingham I, Binas B, Wilde C,
674 Colman A. Lactation is disrupted by α-lactalbumin deficiency and can be restored by
675 human α-lactalbumin gene replacement in mice. Proc Natl Acad Sci U S A.
676 1995;92(7):2835-2839.
677 44. Stephan AB, Shum EY, Hirsh S, Cygnar KD, Reisert J, Zhao H. ANO2 is the cilial
678 calcium-activated chloride channel that may mediate olfactory amplification. Proc Natl
679 Acad Sci U S A. 2009;106(28):11776-11781.
680 45. Stinnakre MG, Vilotte JL, Soulier S, Mercier JC. Creation and phenotypic analysis of
681 alpha-lactalbumin-deficient mice. Proc Natl Acad Sci U S A. 1994;91(14):6544-6548.
682 46. Sudlow AW, Burgoyne RD. A hypo-osmotically induced increase in intracellular Ca^{2+} in
683 lactating mouse mammary epithelial cells involving Ca^{2+} influx. Pflugers Arch.
684 1997;433(5):609-616.
685 47. Sun H, Tsunenari T, Yau KW, Nathans J. The vitelliform macular dystrophy protein
686 defines a new family of chloride channels. Proc Natl Acad Sci U S A.
687 2002;99(6):4008-4013.
688 48. Yang YD, Cho H, Koo JY, Tak MH, Cho Y, Shim WS, Park SP, Lee J, Lee B, Kim BM,
689 Raouf R, Shin YK, Oh U. TMEM16A confers receptor-activated calcium-dependent
690 chloride conductance. Nature. 2008;455(7217):1210-1215.
691
692

692 **Legends**

693

694 **Figure 1. Ca^{2+}-activated Cl^- current in MS cells**

695 ***A-E*:** Representative traces of whole-cell currents of the MS cells. The currents were elicited by
696 the 400-ms voltage steps from −105 mV to +95 mV with 20 mV intervals followed by 400-ms
697 tail potentials of −105 mV (*A*). The cells were perfused with the pipette solution containing
698 different free [Ca^{2+}] of nominally 0 (*B*), 0.1 (*C*) or 1 μM (*D, E*) and with the bath solution richly
699 containing NMDG-Cl (*B-D*) or the NMDG-glutamate (*E*). The data of *D* and *E* were obtained
700 from the same whole-cell configuration. ***F*:** Relationships between current densities and
701 membrane potentials of instantaneous and steady-state currents at 1 μM $[Ca^{2+}]_{pipette}$. The current
702 densities of instantaneous and steady-state currents were measured at 10 and 380 ms of the test
703 pulse (white arrow head and arrow in *A*), respectively. In the inset of *F*, the current densities
704 were normalized by the instantaneous current density at +95 mV in each cell, and the
705 normalized currents were averaged (n = 24). ***G*:** Relationships between steady-state current
706 densities and membrane potentials of MS cells at different $[Ca^{2+}]_{pipette}$. Whole-cell currents at 0,
707 0.1, 0.3, 0.6 and 1 μM $[Ca^{2+}]_{pipette}$ were elicited by the voltage steps (*A*). The steady-state current
708 was measured at 380 ms of the test pulse (arrow in *A*) and normalized by the cell capacitance.
709 Relationship between 1 μM $[Ca^{2+}]_{pipette}$-dependent current that was determined by subtracting
710 the current at 0 μM $[Ca^{2+}]_{pipette}$ from that at 1 μM $[Ca^{2+}]_{pipette}$ and membrane potentials is shown
711 (*G*, inset). ***H*:** Relationships between instantaneous tail current densities and membrane
712 potentials of prepulses at different $[Ca^{2+}]_{pipette}$. The tail current was measured at 10 ms after the
713 onset of the tail potential (arrowhead in *A*) and normalized by the cell capacitance. ***I*:** The
714 relationship between the tail current densities after various prepulse potentials and the
715 concentrations of intracellular Ca^{2+}. ***J*:** Relationships between the normalized Cl^- conductances
716 (g_{Cl}) of the tail currents and the prepulse potentials in various $[Ca^{2+}]_{pipette}$ are summarized. The
717 voltage drop of prepulse potentials and tail potentials due to the series resistance was
718 mathematically collected. Each point represents the mean ± SE (n = 6, 6, 12, 10, and 24 for 0,

719 0.1, 0.3, 0.6 and 1 μM $[Ca^{2+}]_{pipette}$, respectively in Figs. 1*F-J*). The error bars of some data points
720 are hidden behind the graph symbol.
721
722 **Figure 2. Anion selectivity of $I_{Cl\text{-}Ca}$ in MS cells**
723 ***A-D*:** Effects of anion substitution on $I_{Cl\text{-}Ca}$ in the MS cells. The MS cell was perfused with the
724 pipette solution containing 1 μM $[Ca^{2+}]$ and the bath solution richly containing NMDG-Cl. The
725 Cl^- in the bath solution was replaced by I^- (*A*), NO_3^- (*B*), Br^- (*C*) or glutamate (*D*). The currents
726 were elicited by 800-ms ramp pulses from −105 (−104 and −99) to +45 (+46 and +51) mV from
727 the holding potential of −45 (−44 and −39) mV in the NMDG-Cl and -I (-Br and -NO_3, and
728 -glutamate, respectively) bath solution. The current was normalized by that in the NMDG-Cl
729 bath solution at +40 mV in each cell. The averaged normalized currents are show. Insets show
730 the representative *I-V* relationships before and after anion replacement. ***E*:** Permeability ratio to
731 anions. The relative permeabilities of these monovalent anions (P_X-/P_{Cl}-) were estimated using
732 the Goldman, Hodgkin and Katz equation (see Methods and Materials). Data are means ± SE (n
733 = 6, 6, 7 and 6 for I^-, NO_3^-, Br^- and glutamate, respectively)
734
735 **Figure 3. Effects of Cl^- channel blockers on $I_{Cl\text{-}Ca}$ in MS cells**
736 ***A, B*:** The effects of NFA (*A*) and DIDS (*B*) on $I_{Cl\text{-}Ca}$ in the MS cells. The whole-cell currents
737 were recorded with 1000-ms ramp potentials from −105 to +95 mV with the 0.6 μM Ca^{2+}
738 pipette solution in the NMDG-Cl bath solution (Control), the solution with 100 μM NFA or 3
739 mM DIDS and the fresh NMDG-Cl solution (Wash). The currents were normalized by the
740 Control current at +90 mV in the same cell. Each point represents the mean ± SE (n = 5 and 4
741 for NFA and DIDS, respectively). The error bars of some data points are hidden behind the
742 graph symbol. The representative *I-V* relationships of the Control and inhibited currents are
743 shown in the insets. ***C*:** The dose dependency of NFA and DIDS inhibition. The normalized
744 currents at +90 mV with various concentrations of NFA (filled circles) or DIDS (filled

triangles) were plotted. Each point represents the mean ± SE (n = 3-6). The plots were fitted to the Hill equation [$I_{norm} = I_{min} + (1 - I_{min}) / \{1 + ([Inh] / K_d)^h\}$]. ($I_{min} \approx 0.14$, $h \approx 0.8$, and $K_d \approx 3.7$ x 10^{-6} M for NFA. $I_{min} \approx 0.09$, $h \approx 1.5$, and $K_d \approx 805$ x 10^{-6} M for DIDS.) ***D*:** The effect of CaCCinh-A01 on $I_{Cl\text{-}Ca}$ in MS cells. The whole-cell currents were recorded in the NMDG-Cl solution with or without CaCCinh-A01 (100 μM, n = 4) and the averaged normalized currents are shown. Data represent the mean ± SE. The inset shows the representative *I-V* relationships. ***E***: Voltage dependency of inhibitors. The fractions of inhibited current after treatment of NFA (100 μM), DIDS (3 mM), CaCCinh-A01 (100 μM) at −90 and +90 mV are shown. Data represent the mean ± SE (n = 4-5). *, $p < 0.05$ vs. −90 mV.

Figure 4. mRNA expression of CaCCs in lactating mammary glands

A: Schematic diagram of mAno1 gene and TMEM16A protein. White and black boxes represent the constitutive and alternative spliced exons (or protein segments), respectively. Arrows indicate the position of alternative start codon. Bars above the exons indicate the positions where sense (S1-6) and antisense (A1-5) primers bind. ***B*:** mRNA expressions of CaCCs in mammary glands of lactating mice. Total RNA was extracted from the mammary glands of mice at 15 - 18 day of lactation. mRNA expressions of *Ano1*, *Ano2*, *Best1*, *Best2*, *Best3* and *Actb* were examined using RT-PCR in the presence (+) or absence (−) of a reverse transcriptase (RTase). Amplifications obtained from 3 different mice are shown. Positive controls (PC) of the amplification were obtained with total RNA from brain (for *Ano2*) and testis (for *Best2*) of male mice. Scale bars are marked at 100-bp intervals. ***C*:** Transcriptional variants of *Ano1* in the mammary glands of lactating mice. Using various primer pairs, transcriptional variants of *Ano1* were examined. RT-PCR was performed with total RNA obtained from 3 different mice in the presence (+) or absence (−) of RTase. Positive amplifications (PC) were obtained with total RNA from brain of male mice. Arrowheads indicate the positions of the variants. Scale bars are marked at 100-bp intervals.

771

772 **Figure 5. Immunohistochemical staining of TMEM16A in lactating mammary gland**

773 Sections of lactating mammary glands were immunostained with anti-TMEM16A antibody (*A*,
774 *B*) and control IgG (for negative control, *C*). Representative acinar (Ac) and ductal structures
775 (Du) are shown. Arrows indicate the positive staining at apical membrane of MS cells.
776 Arrowheads indicate the intensely stained small epithelial cells. Bars indicate 50 μm.

777

778 **Table 1. Primer pairs for the CaCCs mRNA**

779

780 **Table 2. Primer pairs for the analyses of *Ano1* variants**

781 [*1] Ano1 sequence of NM_178642.5 is a variant including exons coding segment *a* and *c*, but not
782 *b* and *d*.

783 [*2] S6 primer does not detect variants including the exon coding segment *c*.

784 [*3] S5 primer does not detect variants skipping the exon coding segment *c*.

785 [*4] S4 and A3 primers bind to the exon coding segment *b* and *d*, respectively. Thus there is no
786 binding site in the sequence of NM_178642.5.

Figure 1

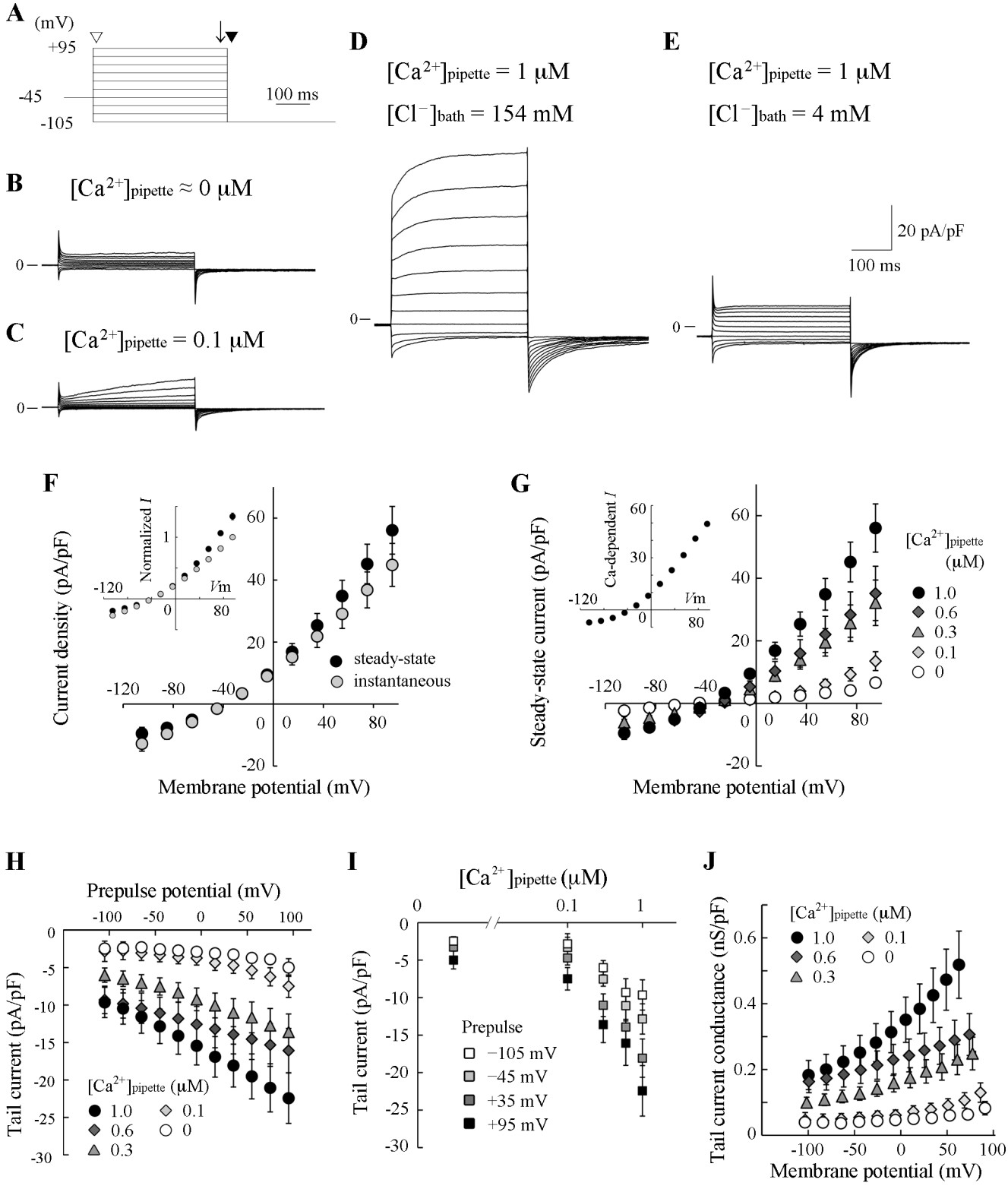
A
(mV)
+95
-45
-105
100 ms
B
[Ca2+]pipette ≈ 0 μM
0
C
[Ca2+]pipette = 0.1 μM
0
D
[Ca2+]pipette = 1 μM
[Cl−]bath = 154 mM
0
E
[Ca2+]pipette = 1 μM
[Cl−]bath = 4 mM
20 pA/pF
100 ms
0
F
Current density (pA/pF)
Normalized I
Vm
steady-state
instantaneous
Membrane potential (mV)
G
Steady-state current (pA/pF)
Ca-dependent I
Vm
[Ca2+]pipette (μM)
1.0
0.6
0.3
0.1
0
Membrane potential (mV)
H
Prepulse potential (mV)
Tail current (pA/pF)
[Ca2+]pipette (μM)
1.0
0.6
0.3
0.1
0
I
[Ca2+]pipette (μM)
Tail current (pA/pF)
Prepulse
−105 mV
−45 mV
+35 mV
+95 mV
J
[Ca2+]pipette (μM)
1.0
0.6
0.3
0.1
0
Tail current conductance (nS/pF)
Membrane potential (mV)

Figure 2

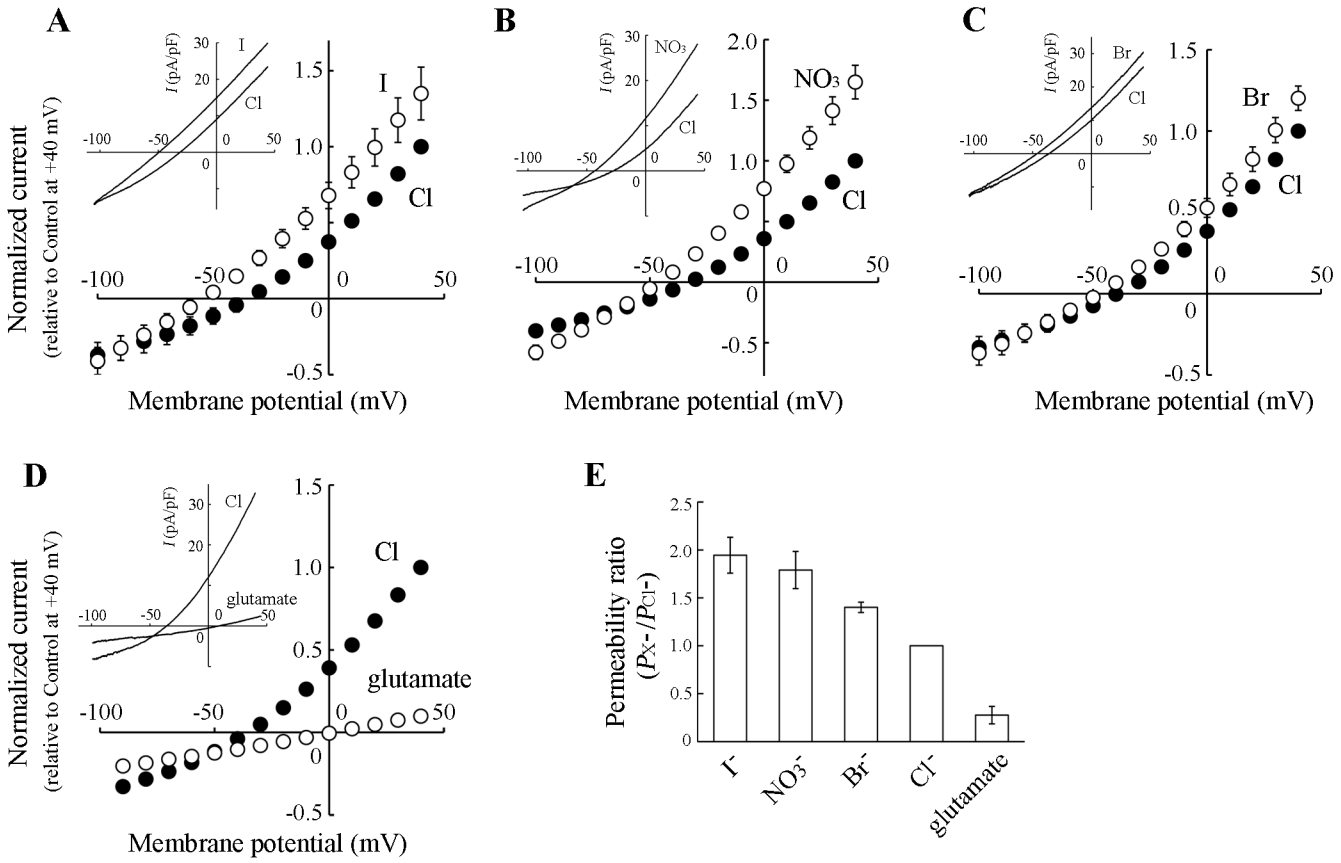
A
B
C
D
E
Normalized current
(relative to Control at +40 mV)
Membrane potential (mV)
I (pA/pF)
I
Cl
NO3
Br
glutamate
Permeability ratio
(PX-/PCl-)
I-
NO3-
Br-
Cl-
glutamate

Figure 3

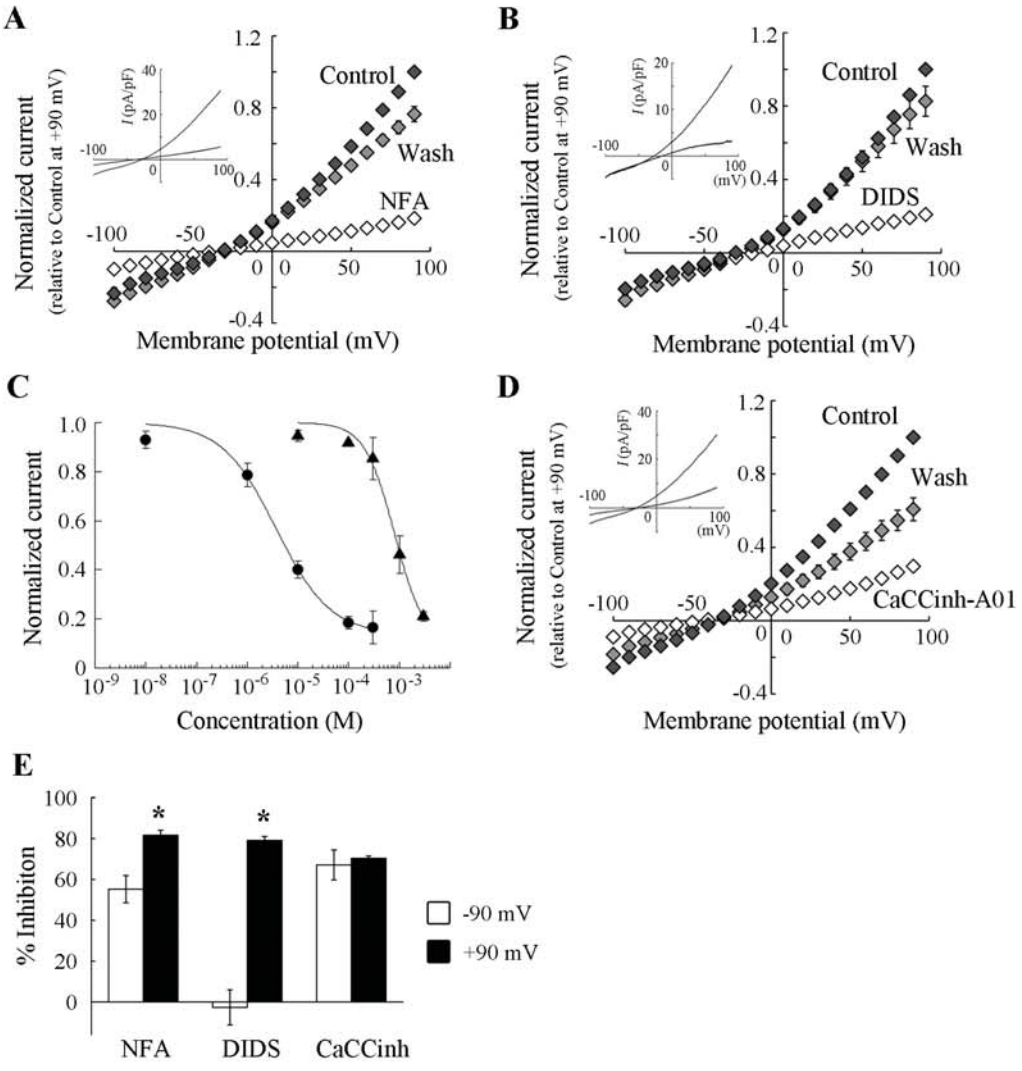
A
Normalized current
(relative to Control at +90 mV)
Control
Wash
NFA
I (pA/pF)
Membrane potential (mV)
B
Normalized current
(relative to Control at +90 mV)
Control
Wash
DIDS
I (pA/pF)
(mV)
Membrane potential (mV)
C
Normalized current
Concentration (M)
D
Normalized current
(relative to Control at +90 mV)
Control
Wash
CaCCinh-A01
I (pA/pF)
(mV)
Membrane potential (mV)
E
% Inhibiton
-90 mV
+90 mV
NFA
DIDS
CaCCinh

Figure 4

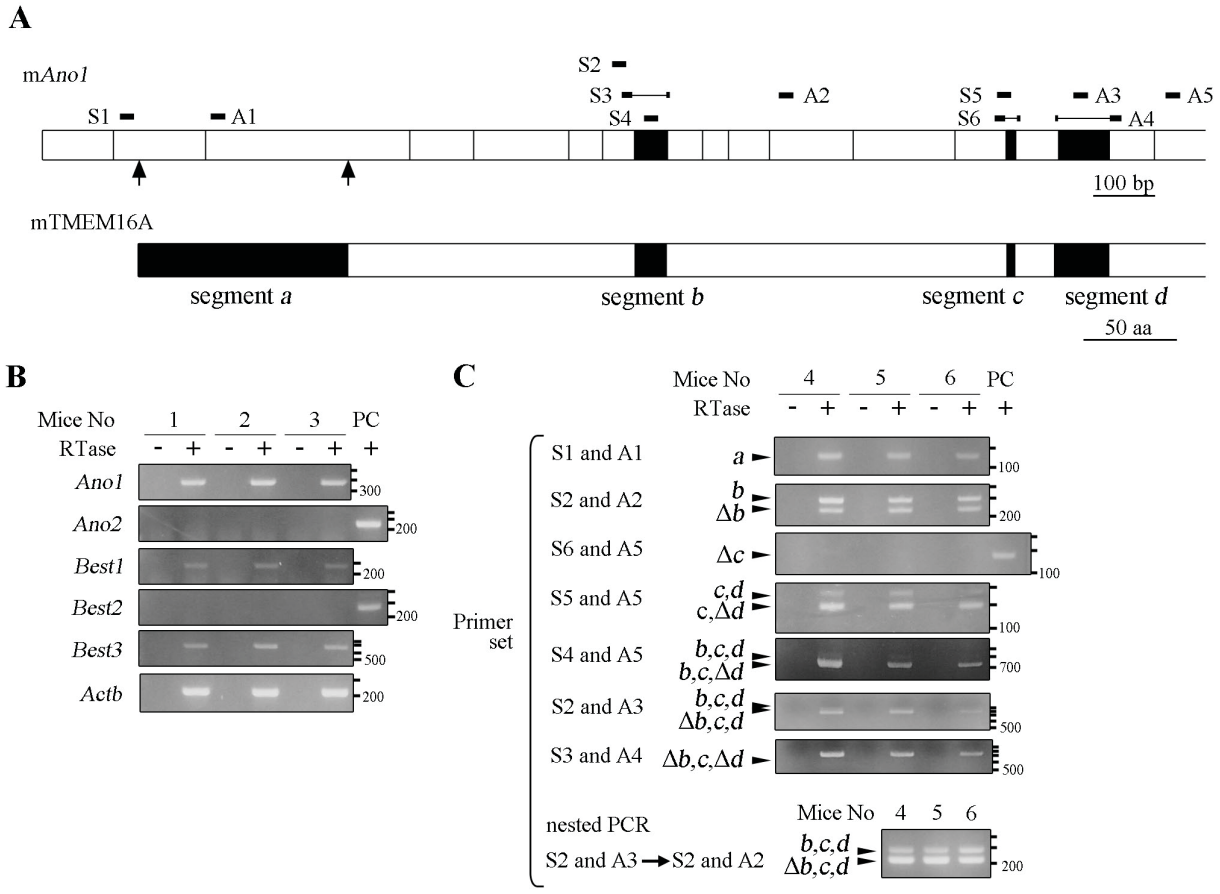
A
mAno1
S1
A1
S2
S3
S4
A2
S5
S6
A3
A4
A5
100 bp
mTMEM16A
segment a
segment b
segment c
segment d
50 aa
B
Mice No
1
2
3
PC
RTase
- + - + - + +
Ano1
Ano2
Best1
Best2
Best3
Actb
300
200
200
200
500
200
C
Mice No
4
5
6
PC
RTase
- + - + - + +
Primer set
S1 and A1
a
100
S2 and A2
b
Δb
200
S6 and A5
Δc
100
S5 and A5
c,d
c,Δd
100
S4 and A5
b,c,d
b,c,Δd
700
S2 and A3
b,c,d
Δb,c,d
500
S3 and A4
Δb,c,Δd
500
nested PCR
S2 and A3 → S2 and A2
Mice No 4 5 6
b,c,d
Δb,c,d
200

Figure 5

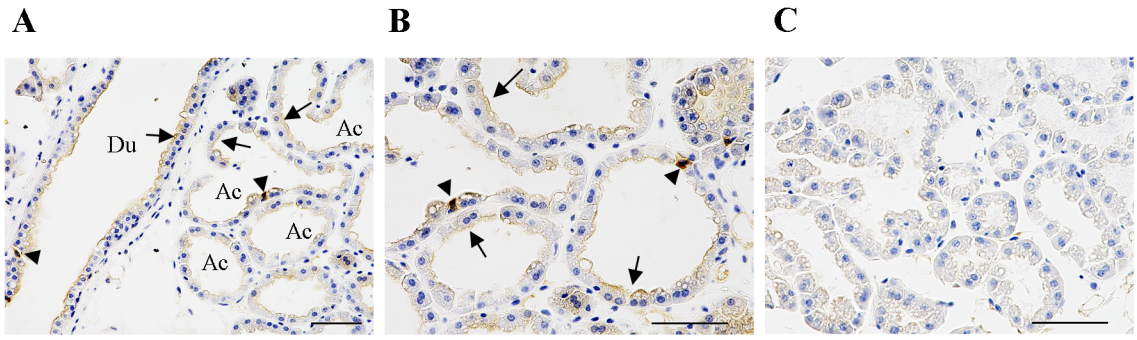

Table 1

Target (Gene name)	Accession No. (Amplified region)	Primer pair	Product size
TMEM16A (*Ano1*)	NM_178642.5 (471-829)	5'- accatcacaagagagcctcag -3' 5'- cgtctcactgatgtggtaca -3'	359 bp
TMEM16B (*Ano2*)	NM_153589.2 (633-881)	5'- gaggcgcacacctgggtcac -3' 5'- atggggcgtggatccggaca -3'	249 bp
Bestrophin1 (*Best1*)	NM_011913.2 (1537-1819)	5'- ttaagggtctggacttcttg -3' 5′- gactctgcatgctccttcat -3'	283 bp
Bestrophin2 (*Best2*)	NM_001130194.1 (84-347)	5'- cgatgaccgtcacctacaca -3' 5′- gagtcacgtagaagccaagta -3'	264 bp
Bestrophin3 (*Best3*)	NM_001007583.1 (2046-2693)	5'- ttctcagcagacagccatcag -3' 5′- ttccatgaaagcccctgtgtg -3'	648 bp
β-actin (*Actb*)	NM_007393.3 (28-246)	5'- cagcttctttgcagctcctt -3' 5′- tcacccacataggagtcctt -3'	219 bp

Table 2

Related segments	Accession No. (Amplified region)	Sense primer (primer name) Antisense primer (primer name)	Predicted product size
seg. *a*	NM_178642.5 [*1] (243-399)	5'- ttgtggatggggagcgcga -3'(S1) 5'- tccacggacagagagttcag-3' (A1)	157 bp
seg. *b*	NM_178642.5 (1032-1262)	5'- agagaacaacgtgcaccaa -3' (S2) 5'- agtacaggccaaccttctca -3' (A2)	231 bp (*b* skipping) 297 bp (*b* inclusion)
seg. *c* & *d*	NM_178642.5 (1595-1790)	5'- ttcgaggaggaggaggatc -3' (S6)[*2] 5'- cgattgcaaatgtcactgcg -3' (A5)	No amplification (*c* inclusion) 184 bp (*c* & *d* skipping) 262 bp (*c* skip, *d* inclusion)
seg. *c* & *d*	NM_178642.5 (1601-1790)	5'- gaggaggaggaagctgtcaa -3' (S5)[*3] 5′- cgattgcaaatgtcactgcg -3' (A5)	No amplification (c skipping) 190 bp (*c* inclusion, *d* skipping) 268 bp (*c* & *d* inclusion)
seg. *b*, *c* & *d*	NM_178642.5 ([*4] -1790)	5'- ctctgcccttctaagtaaacg -3' (S4) 5′- cgattgcaaatgtcactgcg -3' (A5)	No amplification (*b* skipping) 764 bp (*b* & *c* inclusion. *d* skipping) 842 bp (*b*, *c* & *d* inclusion)
seg. *b*, *c* & *d*	NM_178642.5 (1032-[*4])	5'- agagaacaacgtgcaccaa -3' (S2) 5′- ccctctgcttccatttgttg -3' (A3)	No amplification (*d* skipping) 711 bp (*b* skipping & *c*, *d* inclusion) 777 bp (*b*, *c* & *d* inclusion)
seg. *b*, *c* & *d*	NM_178642.5 (1053-1710)	5'- ccaagtacagcatgggtatc -3' (S3) 5'- agcttcaccttgtcggtctc -3' (A4)	No amplification (*b* or *d* inclusion) 658 bp (*b* & *d* skipping, *c* inclusion)